Nuclear Materials and Energy 29 (2021) 101075

Contents lists available at ScienceDirect

Nuclear Materials and Energy

journal homepage: www.elsevier.com/locate/nme

Fabrication and characterization of Cu reinforced with Y-enriched particles following a novel powder metallurgy route

A. Muñoz [a,*], B. Savoini [a], M.A. Monge [a], Y. Ortega [b], O.J. Dura [c]

[a] Universidad Carlos III de Madrid, Departamento de Física, Avda de la Universidad 30, 28911-Leganés, Madrid, Spain
[b] Departamento de Física de Materiales. Facultad de Ciencias Físicas. Universidad Complutense de Madrid, 28040 Madrid, Spain
[c] Universidad de Castilla-La Mancha, Departamento de Fisica Aplicada and INEI, 13071 Ciudad Real, Spain

ARTICLE INFO

Keywords:
Dispersion strengthened copper
Powder metallurgy route
Thermal conductivity of ODS copper
Yttria

ABSTRACT

Dispersion strengthened copper alloys have been produced following an innovative powder metallurgy route. Copper and yttrium acetate powders have been mechanically alloyed and posteriorly thermal treated at 923 K for 3 h and 15 h under a hydrogen atmosphere in order to transform the yttrium acetate into Y_2O_3. Subsequently, the powders were consolidated by hot isostatic pressing. It has been concluded that the duration of the thermal treatment of the powder is a determining factor in the degree of densification of the alloy. The study of the microstructure by Scanning Electron Microscopy and Electron Backscatter Diffraction has revealed the presence of micrometer and submicrometer grains and nanometric Y-O enriched Cu particles embedded in the copper matrix, the mean grain size being smaller for the sample produced from the powder thermal treated for 15 h. Transmission Electron Microscopy investigations concluded that the nanoparticles exhibit a spherical shape with a size up to 25 nm and correspond to monoclinic Y_2O_3. Annealing twins have been also observed, especially in the material produced from thermal treated powder for longer.

The mechanical properties have been inferred from Vickers microhardness measurements and compression tests. Below 473 K the yield strengths of the produced materials are greater than that of pure copper and above 473 K are close to them. From the study of the thermal properties of the densest material it has been found that its thermal conductivity remains nearly constant in the temperature range 300–773 K, and its value is around 85% the thermal conductivity of CuCrZr, the reference material for ITER.

Introduction

Over the past years, some impressive progress has been made on the design of the cooling water system of ITER and the next generation of nuclear fusion reactors [1]. Copper-based alloys are the most promising candidates to be used in the heat-sink systems due to their high thermal conductivity and mechanical properties at moderate temperature [2,3]. In particular, the precipitation hardened alloy CuCrZr has been chosen for high heat flux applications in the water-cooled PFCs designs for ITER [4,5].

CuCrZr will play an important role in the cooling system of the divertor, which is expected to evacuate around 15% of the total fusion power [6,1]. The mechanical properties of CuCrZr below 350 °C are suitable for the ITER requirements, however above 400 °C, the precipitate coarsening and the matrix recrystallization yields to a deterioration of the mechanical strength. A similar softening of the mechanical properties of CuCrZr above 300 °C take place when it is submitted to irradiation [7,4].

A dispersion strengthened (DS) copper alloy can be obtained by the dispersion of fine Y_2O_3 particles. Usually, the mechanical alloying is the most suitable method for achieving a good dispersion of hard particles in a metallic matrix. However, due to the high ductility of copper, the milling process originates the appearance of cold welding phenomena giving place to an agglomeration of the powder particles. Recently, DS Cu-Y_2O_3 and Cu-Y alloys have been produced [8–10]. The cold welding phenomena has been mitigated by either cryogenic milling or decreasing the milling speed and alternating short milling periods with longer repose periods [8]. Also, the stearic acid as a process control agent has been used to avoid cold welding [11,12]. Subsequently, and previously to the sintering process, the powder must be submitted to a thermal treatment in order to eliminate the dispersive agent.

In this research work, a novel fabrication route has been designed for

* Corresponding author.
E-mail address: angel.munoz@uc3m.es (A. Muñoz).

https://doi.org/10.1016/j.nme.2021.101075
Received 21 June 2021; Received in revised form 13 September 2021; Accepted 14 September 2021
Available online 20 September 2021

producing DS Cu-Y_2O_3 [13]. Blends of copper and yttrium acetate ($Y(CH_3CO_2)_3{\cdot}4H_2O$) powders have been mechanically alloyed in a planetary ball milling. The advantages of this method are that yttrium acetate acts as a process control agent (PCA), preventing cold welding and it is the precursor for the formation of the reinforcing particles. Later, the milled powder was subjected to a thermal treatment in a reducing hydrogen-enriched atmosphere, what gave place to the decomposition of yttrium acetate and to the formation of yttrium-enriched particles. This method was already tested in the production of Ni/Y_2O_3 nanocomposites [14]. Subsequently, the powder was consolidated by hot isostatic pressing (HIP) and a study of the microstructure, mechanical properties and thermal conductivity has been carried out.

Experimental procedure

Copper powder with a purity of 99% and yttrium (III) acetate tetrahydrate powder, $Y(OOCCH_3)_3{\cdot}4H_2O$, with a purity of 99.9%, were mixed for 4 h in a Turbula mixer in the proportion of 97 wt% (Cu): 3 wt% ($Y(OOCCH_3)_3{\cdot}4H_2O$). The compositions were adjusted to give a final composition of 1 wt% Y_2O_3 after burn-out of the organic compounds before sintering. The blends were grinded into a planetary ball milling during 72 h at a 150 r.p.m speed, with Cr steel balls, all of them with the same size, 5 mm diameter, being the ball to powder ratio (in mass) of 7:1. Along these processes, the powders were manipulated under an argon protecting atmosphere. Before sintering, the powders were thermal treated at 923 K during 3 h under an Ar-10 vol% H_2 atmosphere to eliminate the organic compounds and induce the formation of Y_2O_3. Another batch of powder was milled following the same process, but with 15 h of thermal treatment. Both powder batches were encapsulated into steel cans and degassed in vacuum for 24 h at 573 K. Later, the powders were sintered by high isostatic pressing, HIP, at 1173 K during 3 h under a 180 MPa pressure. The resulting materials were denoted as Cu-1Y3 and Cu1Y15, in correspondence with the duration of the thermal powder treatment.

X-Ray diffraction patterns were recorded along the different steps of the fabrication process and the crystallite size and internal stress of the powder were evaluated using the Fullprof software and the Rietveld method [15]. The density of the consolidated alloys was determined by using a He ultrapycnometer. The study of the microstructure was carried out with a high resolution scanning microscope (SEM) FE-SEM FEI TENEO, equipped with a X-Ray energy dispersive detector and a scanning microscope SEM-FEG JEOL JSM 6500F equipped with an EBSD detector. The EBSD patterns were analyzed using the MTexv3.2.5 data analysis software [16]. In order to discriminate the grain boundaries, it was considered an angle of crystallographic misorientation between adjacent crystalline domains larger than 5°. The experimental grain size distributions were determined from electron channeling contrast (ECC) images using an improved approach of the Jhonson–Saltykov stereological method that enables to obtain the spatial grain size distribution of the 3D microstructure from 2D grain size measurements [17]. Cu1Y15 sample for transmission electron microscopy (TEM) observations was prepared by focused ion beam (FIB). TEM investigations were performed in a JEOL JEM 2100 at 200 kV.

The mechanical properties of the alloys were obtained from Vickers microhardness measurements at room temperature and compression tests in the temperature range 300–773 K. For the microhardness measurements a load of 9.81 N was applied during 20 s. The compression tests were performed at a strain rate of $1.0x10^{-4}$ s^{-1} on cylindrical samples 9 mm height and 5 mm diameter.

A characterization of the thermal properties of Cu-1Y15 was also performed. Firstly, the thermal diffusivity, α, was measured from 323 K to 773 K by the laser flash method, using a Linseis (Linseis Messgeraete GmbH, Germany) LFA 1000 instrument under an Ar atmosphere. Previously, the sample, with a size of $9.5 \times 9.5 \times 1$ mm^3, was covered with a thin graphite layer to ensure the full absorption of the flash light at the front surface and a high emissivity from the back side. Secondly, the specific heat, Cp, was obtained over the temperature range 323–773 K using a Netzsch Jupiter DSC 404 differential scanning calorimeter (Netzsch-Gerätebau GmbH, Germany), Pt crucibles and a scan rate of 20 $Kmin^{-1}$. For these measurements, the samples were disc-shaped with a diameter of 5 mm and 1 mm of thickness. A single crystal of sapphire was used as a reference material. Finally, the thermal conductivity, λ, was determined from the separate measurements of α, C_p, and ρ, according to the expression: $\lambda = \alpha \bullet C_p \bullet \rho$ where ρ denotes the density of the sample.

Results and discussion

Powder characterization

The copper particles of the initial powder had sizes between 4 and 150 μm. After 72 h of milling the particles took a flake shape with sizes below 20 μm (see Fig. 1). The normalized X-Ray diffraction patterns of the powder along the different steps of the fabrication process are shown in Fig. 2. The characteristics Bragg peaks associated to copper are clearly observed in all the X-Ray patterns. Also, some peaks related to Yttrium acetate are observed in the X-Ray pattern of the mixed powder in the range 25–40°. The strongest Bragg peak of Cu_2O is observed in the pattern of the powder milled during 72 h (Fig. 2 inset), however in the X-Ray patterns corresponding to the powder thermal treated in a hydrogen atmosphere, it is appreciated the presence of CuO. During the milling process, the most important source of oxygen comes from the dehydratation and decomposition of the yttrium acetate tetrahydrate into Y_2O_3 following the reactions [18,19]:

$$Y(CH_3CO_2)_3 \bullet 4H_2O \rightarrow Y(CH_3CO_2)_3 + 4H_2O \quad (1)$$

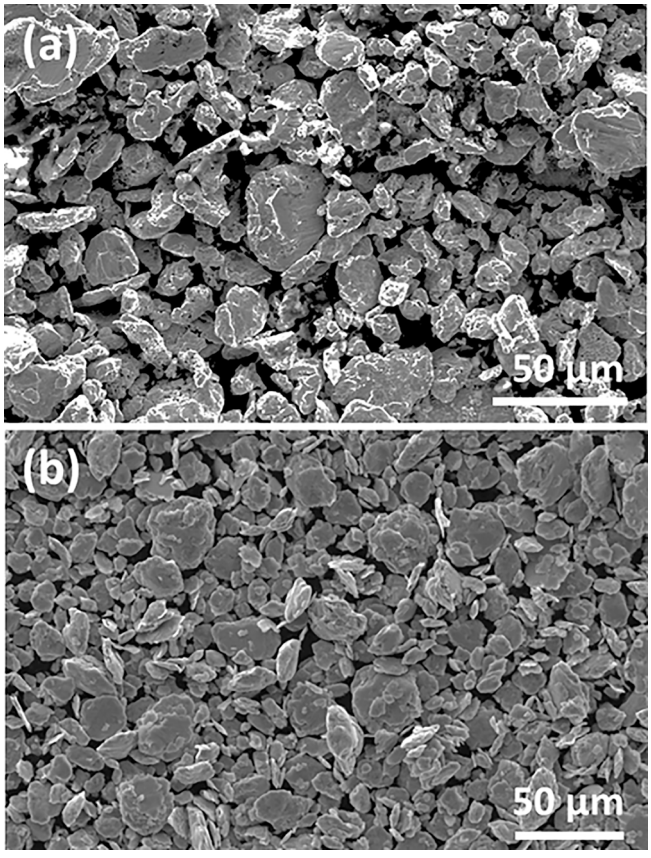

Fig. 1. SEM images of the powder. (a) Initial raw powder after mixing. (b) Powder after milling in the planetary ball milling during 72 h.

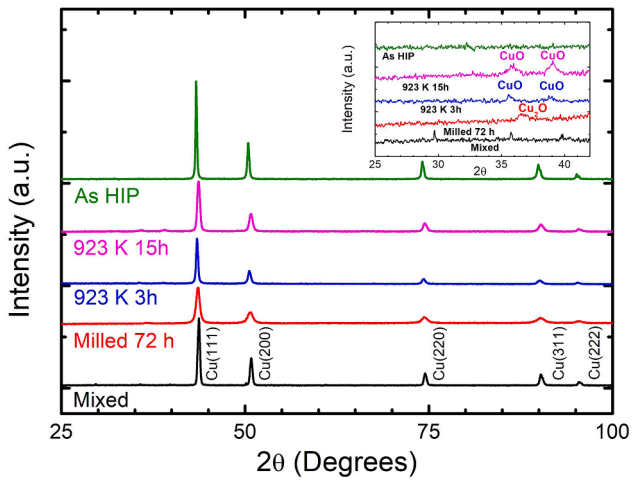

Fig. 2. Normalized X-Ray diffraction patterns of the alloys along the different steps of the production route. Black line (mixed powder); red line (Cu-1Y15 milled powder; the corresponding Cu-1Y3 pattern is similar); blue line (Cu-1Y3 powder after milling + treatment in H_2); pink line (Cu-1Y15 powder after milling + treatment in H_2) and green line (Cu-1Y15 after HIP; the corresponding Cu-1Y3 pattern is similar). The inserted figure is an enlargement of the angular region 25–42°. (For interpretation of the references to colour in this figure legend, the reader is referred to the web version of this article.)

$$Y(CH_3CO_2)_3 \rightarrow \frac{1}{2}Y_2O_2CO_3 + CO_2 + \frac{3}{2}CH_3COCH_3 \quad (2)$$

$$Y_2O_2CO_3 \rightarrow Y_2O_3 + CO_2 \quad (3)$$

starting the first reaction at 323 K, the second at 653 K and the third one at 863 K. In presence of copper some of the products of the reactions could give place to Cu_2O and CuO. As the enthalpy of formation of Cu_2O is more negative (−170.71 kJ/mol) than that of CuO (−150.06 kJ/mol) [20], it is expected that the amount of Cu_2O in the powder is greater than that of CuO, in agreement with the results observed in the X-Ray pattern after milling. These copper oxides would again transform into Cu through the reactions:

$$Cu_2O + H_2 \rightarrow 2Cu + H_2O \quad (4)$$

$$CuO + H_2 \rightarrow Cu + H_2O \quad (5)$$

However, X-Ray measurements show that a thermal treatment at 923 K in a hydrogen atmosphere, even after 15 h, is not able to transform all the CuO into Cu (inset of Fig. 2), since a certain amount of copper oxide still remains in the powder.

The effect of the milling process in the crystallite size and the internal stresses is presented in Fig. 3. The size of the crystallite size seems to stabilize after 56 h milling, whereas the internal strains increase on increasing the milling time, although they remain stable after 64 h. Therefore, these results indicate that around 60 h would be and appropriate milling time for a 150 rpm milling velocity. However, in order to facilitate the comparation, the powders of both batches were milled during the same time, 72 h, in the planetary ball milling.

Microstructure

The density of the consolidated alloys Cu-1Y3 and Cu1-Y15 has been evaluated with a He ultra-pycnometer and compared with the theoretical value. The theoretical value has been calculated using the phases rule, assuming that all the yttrium has been transformed into Y_2O_3, so that the theoretical composition of the alloy is Cu-1 wt%Y_2O_3. For the densities of Cu and Y_2O_3 the values of 8.96 and 5.01 g/cm^3 have been used, respectively. As it is shown in Table 1, the degree of densification of Cu-1Y3 and Cu-1Y15 is 92.6 ± 0.1% and 96.8 ± 0.1%, respectively.

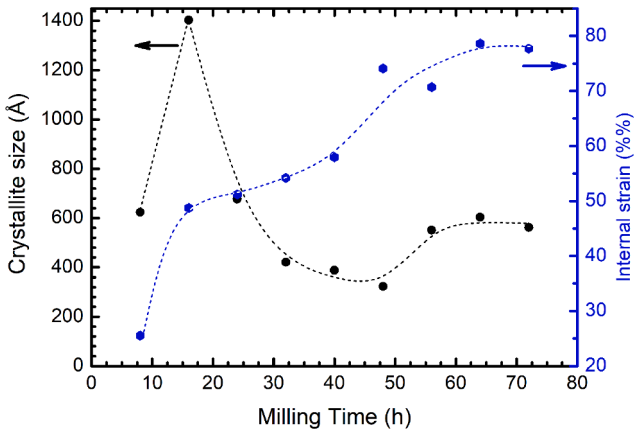

Fig. 3. Evolution of the crystallite size and internal stress of the Cu-1Y3 powder with the milling time.

Table 1
Density, average grain size and Vickers microhardness of the Cu-1Y3 and Cu-1Y15 alloys.

Sample	Density (g/cm^3)	Densification (%)	Average grain size (μm)	Grains with twins (%)	Vickers microhardness (GPa)
Cu-1Y3	8.23 ± 0.01	92.6 ± 0.1	0.9 ± 0.5	49.9	1.57 ± 0.07
Cu-1Y15	8.61 ± 0.01	96.8 ± 0.1	0.7 ± 0.4	58.7	1.85 ± 0.03

The X-Ray pattern of the consolidated Cu-1Y15 is presented in Fig. 2 and only the Bragg peaks associated to copper are observed. The same result is obtained for Cu-1Y3 (the X-Ray pattern is not presented for clarity reasons). CuO, which was present after the last thermal treatment of the powder, is not observed after consolidation. As the melting (1599 K) and boiling points (2273 K) of CuO are far away from the degassing, 573 K, and the HIP, 1173 K, temperatures, appears reasonable that Y-O rich particles (not detected within the X-ray equipment resolution) could have formed during the sintering process.

The microstructure of the Cu-1Y3 and Cu-1Y15 alloys after consolidation by HIP is shown in Fig. 4a and c, respectively. In both samples, the grains of the copper matrix are equiaxed, with sizes both in the submicrometer and micrometer range. Twins are also observed in the micrometric grains. The dark areas presented in the micrographies correspond to cavities, exhibiting Cu-1Y3 a higher density of cavities than Cu-1Y15, in good agreement with the experimental density values. Fig. 4b and d show enlarged areas of submicrometer-grain regions, where nanometric yttrium-oxygen enriched particles (marked with arrows) can be observed.

To identify the nature and structure of these Y-O enriched nanoparticles, TEM investigations were performed on the Cu-1Y15 sample. Low-magnification TEM images of different regions of the sample, as the one observed in Fig. 5(a), show that the nanoparticles exhibit a spherical shape, and sizes up to 25 nm. The analysis of HRTEM images of single nanometric particles, as the one shown in Fig. 5(b) enabled to assess their crystalline structure. The interplanar distance of lattice fringes depicted in Fig. 5(c) corresponds to the (202) crystal planes of the Y_2O_3 monoclinic structure and moreover, the fast Fourier transform (FFT) of this area reveals diffractions associated with the (202), (313) and (111) planes of that same crystalline phase (Fig. 5d). Therefore, TEM results enabled to identify the nature of these nanometric particles as monoclinic Y_2O_3 phase.

The microstructure of the alloys has also been analyzed by EBSD measurements. The orientation image micrographs (OIMs) obtained in

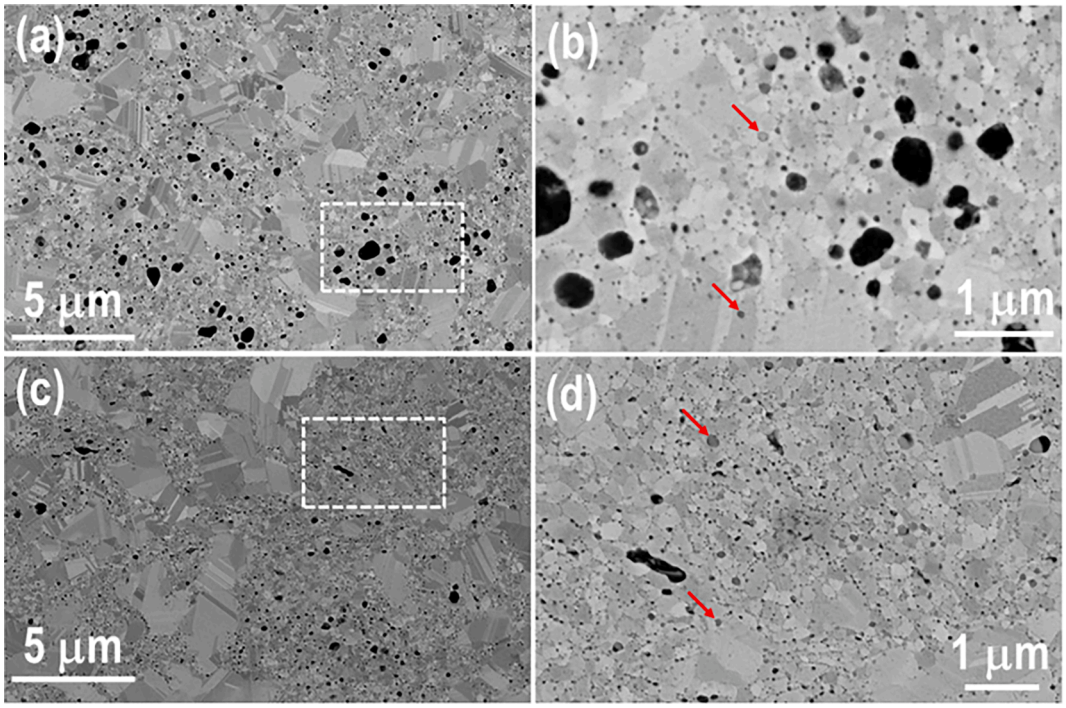

Fig. 4. SEM images of the microstructure of Cu-1Y3 (a) and Cu-1Y15 (c). The images (b) and (d) correspond to an enlargement of a region (marked with a dot line) of images (a) and (c), respectively.

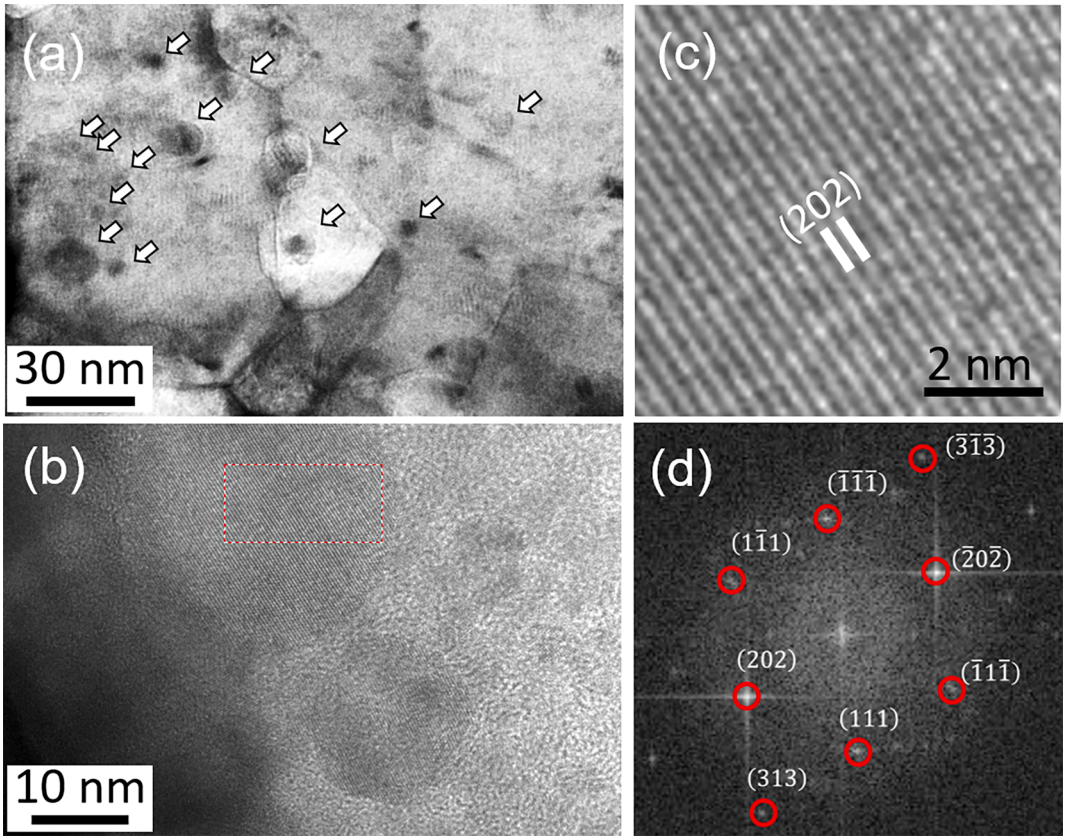

Fig. 5. (a) Low-magnification TEM image of Cu1-Y15 showing spherical nanoparticles. (b) HRTEM image of nanoparticles. (c) Lattice fringes of the HRTEM image correspond to the (2 0 2) crystal planes of Y_2O_3 monoclinic phase. (d) The corresponding FFT pattern shows reflections of Y_2O_3 monoclinic structure.

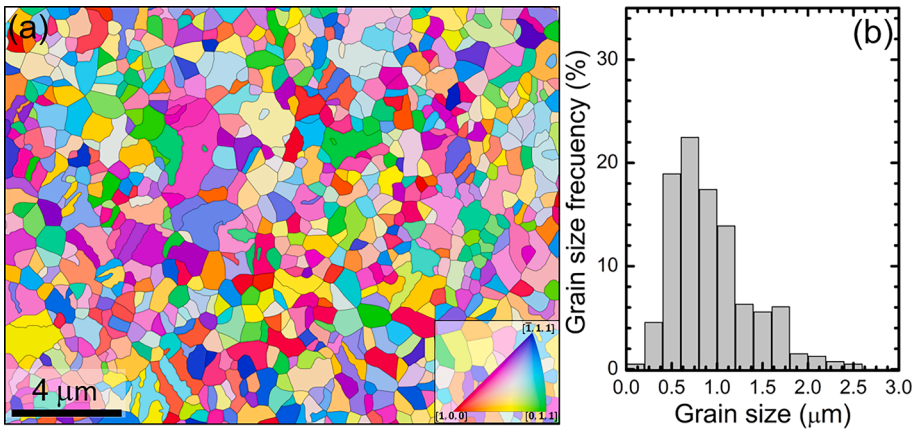

Fig. 6. (a) Inverse pole figure map showing the microstructural features of Cu-1Y3. (b) Grain size distribution of Cu-1Y3.

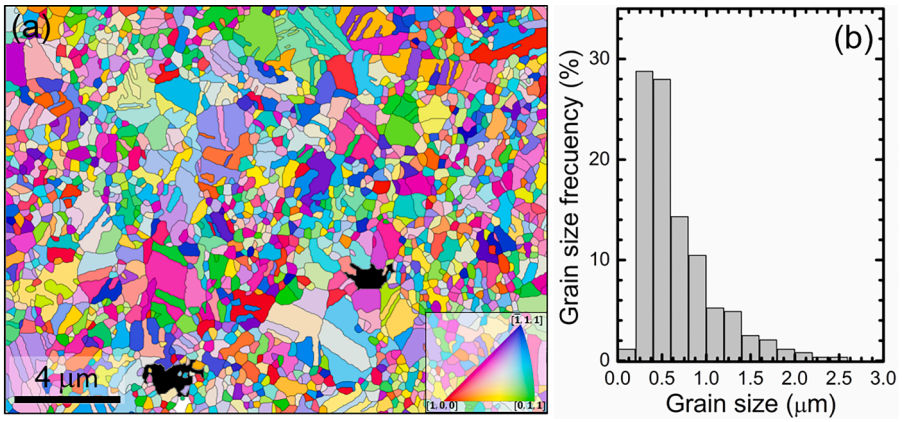

Fig. 7. (a) Inverse pole figure map showing the microstructural features of Cu-1Y15. (b) Grain size distribution of Cu-1Y15. Dark regions correspond to cavities.

the study are shown in Fig. 6a for Cu-1Y3 and 7a for Cu-1Y15, and the calculated grain size distributions are displayed in Fig. 6b (Cu-1Y3) and Fig. 7b (Cu-1Y15).

According to Figs. 6 and 7, both alloys present equiaxed grains but the grain size is smaller for Cu-1Y15, with mean grain sizes of 0.9 ± 0.5 and 0.7 ± 0.4 μm for Cu-1Y3 and Cu-1Y15, respectively (see Table 1). Another important feature is the presence of a higher number of annealing twins in the Cu-1Y15 sample, which were formed in the course of the recrystallization process that occurs during the sintering by HIP. From the OIM images the fraction of grains containing twins has been evaluated, resulting in values of ~50 and ~59% for Cu-1Y3 and Cu-1Y15, respectively (see Table 1). The only difference in the fabrication of both alloys was the duration of the thermal treatment (3 h for Cu-1Y3 and 15 h for Cu-1Y15) that was performed to the powder before the sintering process. The formation of annealing twins during the recrystallization process is linked to the stacking fault energy, and it is known that the smaller the stacking fault energy the more twins are observed. In FCC metals the stacking fault energy decreases on increasing the concentration of solute in the matrix. It would mean that the presence of solute in Cu-1Y15 would be greater than in Cu-1Y3. The powder used for

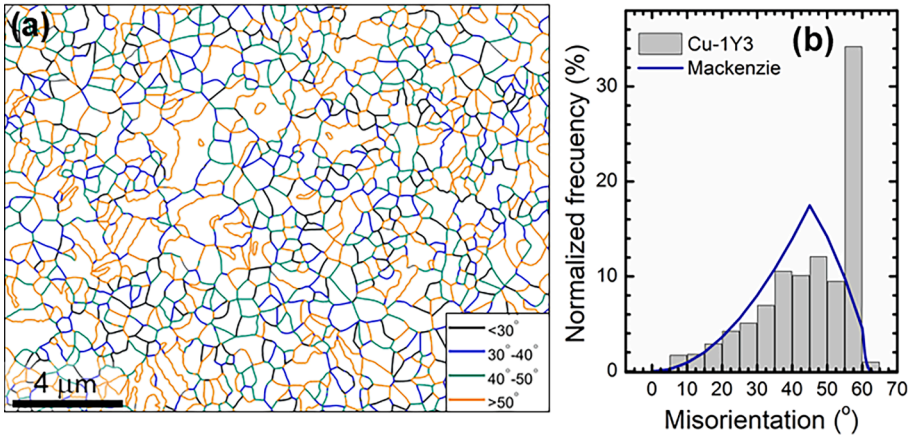

Fig. 8. (a) Grain boundaries misorientation of Cu-1Y3. The analysis was performed in the micrograph showed in Fig. 6. (b) Corresponding misorientation distribution. The Mackenzie's distribution is also depicted.

the Cu-1Y15 was submitted to a thermal treatment 5 times longer than that of the Cu-1Y3, so it is expected that more Y_2O_3 particles were formed in the former according to the dehydratation and decomposition reactions (1–3). This would also explain that the grain size was smaller for Cu-1Y15, since the presence of these oxides in the copper matrix would prevent the growing of the grains during the recrystallization.

The grain misorientation for Cu-1Y3 and Cu-1Y15 is represented in Figs. 8 and 9 where it can be observed that for both materials the macrotexture is negligible, as the distributions are very similar to the Mackenzie one, which corresponds to that expected in absence of crystallographic texture or twining. The only exception is found at 60°, which corresponds to the primary copper annealing twins 60° ⟨1 1 1⟩ .

Mechanical properties

The Vickers microhardness values measured at room temperature are shown in Table I. The microhardness is greater for Cu-1Y15, 1.85 GPa, than for Cu-1Y3, 1.57 GPa, which is attributed to its higher densification. These microhardness values are greater than that of pure copper, 0.369 GPa [21], indicating that a reinforcement of the copper matrix has taken place. On the other hand, these values (189 ± 3 HV for Cu-1Y15 and 160 ± 7 HV for Cu-1Y3) are close to the values of the GlidCop alloys and other ODS Cu-Y_2O_3 alloys obtained following different routes [22,10].

The results obtained in the compression tests carried out from RT to 753 K are presented in Fig. 10. As it can be appreciated, the mechanical strength is greater for Cu-1Y15 than for Cu-1Y3, what is meanly due to the difference in the degree of densification. The evolution of yield strength with the temperature is presented in Fig. 11, along with the corresponding value for pure copper found in the literature [23]. Cu-1Y15 exhibits a slightly higher yield strength value than Cu-1Y3. Below 473 K the yield strength is much higher for the Cu-1Y3 and Cu-1Y15 alloys than for pure copper, however above 473 K the yield strength of the alloys slumps to values close to the corresponding values of pure copper, in concordance with the drop observed at this temperature in the compression curves. The yield strength depends on different factors as the dislocation density, the grain size and the presence of impurities and precipitates. On the one hand, Cu-1Y15 exhibits a smaller grain size than Cu-1Y3 and, on the other hand, the higher duration of the thermal treatment under a hydrogen atmosphere performed on Cu-1Y15 before sintering, can give place to a higher density of hard Y_2O_3 particles in Cu-1Y15. Therefore, both factors can explain that Cu-1Y15 exhibits a greater yield strength than Cu-1Y3.

The behavior of the yield strength of Cu-1Y3 and Cu-1Y15 above 473 K can be explained by the appearance of a dynamic recrystallization. This phenomenon is usually observed in copper [24] and it occurs during the metal deformation at high temperature and it is associated to the nucleation of new grains with a low density of dislocations and their subsequent growth. The compression curves presented in Fig. 10 present and important decreasing in the mechanical strength above 473 K which is reflected in an important drop in the yield strength. During the compression tests the samples are submitted to a deformation and as it is performed at a temperature close to the recrystallization temperature, the nucleation and grow of new grains with a lower dislocation density can occur. So, the same strain values can be produced with lower stress values.

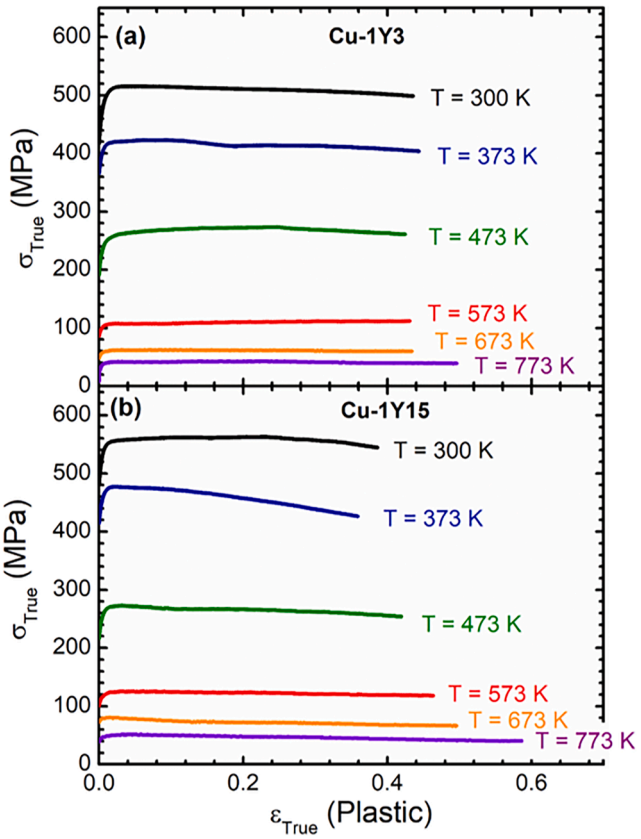

Fig. 10. True strain versus true plastic deformation of (a) Cu-1Y3 and (b) Cu-1Y15 obtained from compression tests at different temperatures.

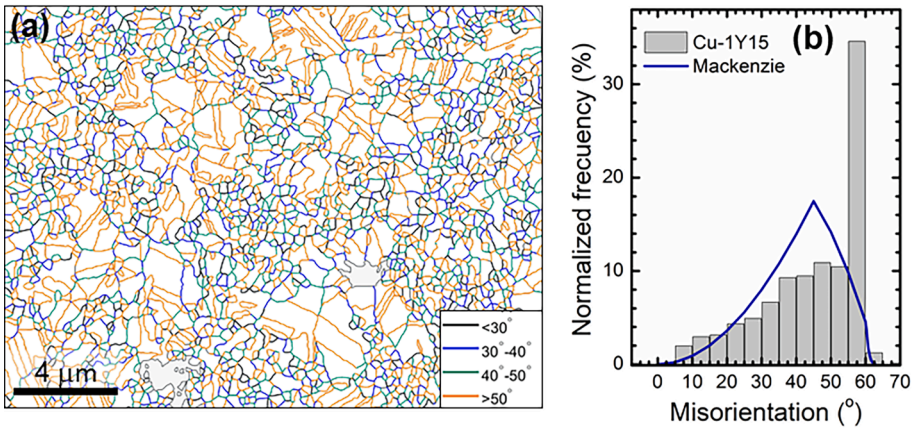

Fig. 9. (a) Grain boundaries misorientation of Cu-1Y15. The analysis was performed in the micrograph showed in Fig. 7. (b) Corresponding misorientation distribution. The Mackenzie's distribution is also depicted.

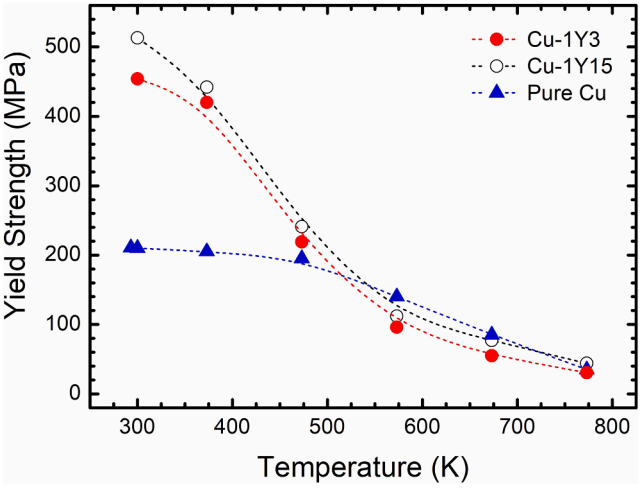

Fig. 11. Evolution of the yield strength with the temperature for Cu-1Y3 (red circle) and Cu-1Y15 (open circle). The yield strength for pure copper is also presented (blue triangle). (For interpretation of the references to colour in this figure legend, the reader is referred to the web version of this article.)

Thermal conductivity measurements

The thermal properties of the Cu-1Y15 alloy in the temperature range RT-773 K have been inferred from the measurements of the thermal diffusivity and specific heat. The thermal diffusivity in a material characterizes the speed of propagation of heat during a change of temperature over time, so it is related to the speed for achieving the thermal equilibrium under variable thermal conditions. The thermal evolution of the thermal diffusivity and specific heat of Cu-1Y15 are shown in Fig. 12(a). The values are compared with those found in the literature for pure copper [25,26]. The specific heat of Cu-1Y15 is very similar to the specific heat of pure copper. It means that the capacity of storing energy in Cu-1Y15 hardly changes on introducing around 1 wt% of Y_2O_3 particles. Let us point that something similar happens for the specific heat of other copper-based alloys as Cu-0.25%Al_2O_3 (GlidCop) and CuCrZr, the reference alloy for ITER [27]. Therefore, when a small percentage of other phase is added to pure copper, the specific heat of the composite continues being meanly associated to the copper matrix.

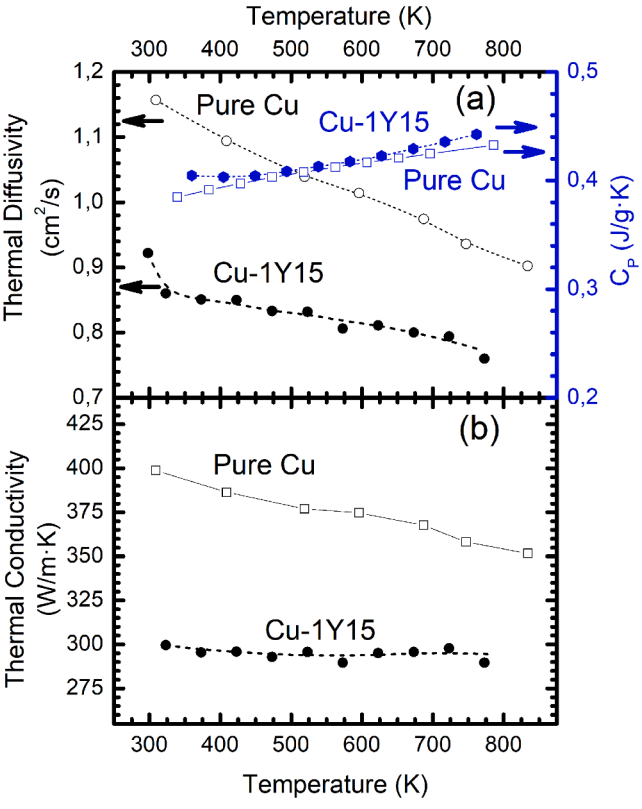

Fig. 12. (a) Thermal diffusivity and specific heat, C_P, of Cu-1Y15 in the temperature range 300–773 K. For comparison, the thermal diffusivity and specific heat of pure copper are also presented. (b) Thermal conductivity of Cu-1Y15 in the temperature range 300–773 K. The thermal conductivity of pure Cu is also presented.

On the other hand, the thermal diffusivity values for Cu-1Y15 are lower than those of pure copper and diminish on increasing the temperature, as it is also observed in pure copper. The thermal diffusivity is a physical quantity defined as the ratio between the thermal conductivity and the heat capacity. In this case, in which the specific heat of Cu-1Y15 is close to that of pure copper, is the thermal conductivity that determines the decrease in the thermal diffusivity. Let us point that, from an experimental point of view it is easier to measure the thermal diffusivity than the thermal conductivity. Due to this fact, the thermal conductivity has been obtained indirectly from the thermal diffusivity. Therefore, the factors that affect to the thermal conductivity in Cu-1Y15 are responsible of the decrease in the thermal diffusivity.

The thermal evolution of the thermal conductivity of Cu-1Y15 is compared with that of pure copper in Fig. 12(b). At room temperature the thermal conductivity of Cu-1Y15 is around 75% that of pure copper (~400 $Wm^{-1}K^{-1}$) and at 773 K is around 81%. It means that a significant reduction is found for Cu-1Y15. Something similar occurs when it is compared with the thermal conductivity of CuCrZr, ~350 $Wm^{-1}K^{-1}$ at room temperature, in this case the reduction is around 85%. The thermal conductivity in a metal is associated to the thermal energy transported by the electrons and the phonons, although due to the great density of electrons most part of the energy is transported by the electrons. However, on increasing the temperature the electron–phonon scattering increases and the lattice contribution to the thermal contribution becomes important. In the metal alloys and composites, the reduction in the thermal conductivity is meanly due to the interaction of the electrons and phonons with the defects which are present in the material. These defects are the grain boundaries, voids and the interface reinforced particle-copper matrix. The degree of densification in Cu-1Y15 is around 97%, so the presence of voids, even if they are of a micrometer size cannot explain by themselves the significant reduction of the observed thermal conductivity. So, the important reduction in the thermal conductivity must be attributed to the scattering of the electrons and phonons with the grain boundaries and with the reinforced particles. Let us point out that it has been observed a great reduction of the thermal conductivity in nanocrystalline copper materials because of the great number of grain boundaries [28]. Cu-1Y15, with an average grain size of 0.7 ± 0.4 μm, cannot be considered as a nanomaterial, but it cannot be disregarded that the reduced grain size plays an important role in the thermal conductivity diminution.

Conclusions

Dispersion strengthened copper alloys have been produced by following a powder metallurgy route, whose first step has been the mechanical alloying of copper and yttrium acetate ($Y(CH_3CO_2)_3{\cdot}4H_2O$) powders. The yttrium acetate has acted as a process control agent, preventing cold welding and facilitating the dispersion of $Y(CH_3CO_2)_3$ in the copper matrix. After the milling process, a thermal treatment under a hydrogen atmosphere has been applied in order to eliminate the volatile compounds and promote the formation of Y_2O_3 particles. The powders were consolidated by high isostatic pressing and a study of the microstructure, mechanical and thermal properties has been carried out. The conclusions derived from this research work are the following ones:

It is possible to obtain DS Cu-Y alloys by mechanical alloying copper

and yttrium acetate ($Y(CH_3CO_2)_3{\cdot}4H_2O$) powders and subsequent sintering by HIP. However, after mechanical alloying, the powders must be submitted to a thermal treatment under a hydrogen atmosphere at 923 K. The duration of this thermal treatment has a strong influence in the degree of densification of the alloy. A thermal treatment of 15 h allows achieving a densification of around 97%.

The study of the microstructure by SEM has revealed the presence of grains with sizes of a few micrometers and also with sub-micrometer size. A significant number of micrometer-sized voids have been observed, which is in good agreement with the results of the density measurements. The pores are surely originated by the volatile compounds formed as a result of the decomposition of yttrium acetate during the thermal treatment that remains trapped inside the copper powder particles. Its number is greater for Cu-1Y3 than for Cu-1Y15, indicating the duration of the thermal treatment of the powder is important for diminishing the porosity.

From the SEM study of the microstructure, it has also been inferred the presence of Y-O rich particles of nanometric size in the copper matrix. It indicates that this fabrication method allows attaining DS copper alloys.

From the TEM study the structure of the Y-O enriched nanoparticles was identified as monoclinic Y_2O_3. They present a characteristic spherical shape with sizes ranging from few nanometers to ~25 nm.

The study of the microstructure by the EBSD technique has shown that the average grain size is smaller for Cu-1Y15 than for Cu-1Y3. In the same way it has been determined that the percentage of annealing twins present in Cu-1Y15 is greater than in Cu-1Y3. All these results indicate that the duration of the thermal treatment of the powder before the sintering process plays an important role in the formation of reinforcing particles in the copper matrix. The more the duration time, the more number of reinforcing particles are formed. It also contributes to the decreasing of the grain size.

The compression tests have revealed that the yield strength of Cu-1Y3 and Cu-1Y15 are greater than that of copper at temperatures below 473 K. Above 473 K the yield strength of these new alloys is close to the value of pure copper.

The thermal conductivity of Cu-1Y15 remains nearly constant in the temperature range 300–773 K. On comparing at room temperature, the thermal conductivity of Cu-1Y15 with that of pure copper and CuCrZr, it results that the thermal conductivity of Cu-1Y15 is around 75% that of pure copper and 85% that of CuCrZr. This significant reduction is meanly associated to the electron and phonon scattering with the grain boundaries and with the interfaces reinforcing particles-copper matrix.

CRediT authorship contribution statement

A. Muñoz: Conceptualization, Methodology, Data curation, Resources. **B. Savoini:** Conceptualization, Methodology, Resources, Writing – review & editing, Supervision. **M.A. Monge:** Conceptualization, Methodology, Software, Resources, Writing - review & editing, Funding acquisition, Supervision. **Y. Ortega:** Conceptualization, Methodology, Software, Resources, Writing - review & editing. **O.J. Dura:** Conceptualization, Methodology, Software, Resources, Writing - review & editing.

Declaration of Competing Interest

The authors declare that they have no known competing financial interests or personal relationships that could have appeared to influence the work reported in this paper.

Acknowledgements

The present work has been supported by the Agencia Estatal de Investigación (PID2019-105325RB-C33 / AEI / 10.13039/501100011033) and by the Regional Government of Madrid through the program TECHNOFUSIÓN(III)CM (S2018/EMT-4437). The support of the Regional Government of Madrid through the multi-annual agreement with UC3M ("Excelencia para el Profesorado Universitario" - EPUC3M14) - Fifth regional research plan 2016-2020 is acknowledge.

Data availability statement

The raw/processed data required to reproduce these findings cannot be shared at this time due to technical or time limitations.

References

[1] P. Norajitra, S.I. Abdel-Khalik, L.M. Giancarli, T. Ihli, G. Janeschitz, S. Malang, I. V. Mazul, P. Sardain, Divertor conceptual designs for a fusion power plant, Fusion Eng. Des. 83 (7-9) (2008) 893–902, https://doi.org/10.1016/j.fusengdes.2008.05.022.

[2] S. J. Zinkle, Applicability of copper Alloys for DEMO high heat flux components, Phys. Scr. T167 (2016) 014004 (10pp). https://doi.org/10.1088/0031-8949/2015/T167/014004.

[3] J.H. You, Copper matrix composites as heat sink materials for water-cooled divertor target, Nucl. Mater. Energy 5 (2015) 7–18, https://doi.org/10.1016/j.nme.2015.10.001.

[4] S.A. Fabritsiev, S.J. Zinkle, B.N. Singh, Evaluation of copper alloys for fusion reactor divertor and first wall components, J. Nucl. Mater. 233–237 (1996) 127–137, https://doi.org/10.1016/S0022-3115(96)00091-8.

[5] D. Stork, et al., Materials R&D for a timely DEMO: key findings and recommendations of the EU roadmap materials assessment group, Fusion Eng. Des. 89 (2014) 1586–1594, https://doi.org/10.1016/j.fusengdes.2013.11.007.

[6] J.H. You, E. Visca, C.h. Bachmann, T. Barrett, F. Crescenzi, M. Fursdon, H. Greuner, D. Guilhem, P. Languille, M. Li, S. McIntosh, A.V. Müller, J. Reiser, M. Richou, M. Rieth, European DEMO divertor target: operational requirements and material-design interface, Nucl. Mater. Energy 9 (2016) 171–176, https://doi.org/10.1016/j.nme.2016.02.005.

[7] M. Li, S.J. Zinkle, Physical and mechanical properties of copper and copper alloys, Comprehen. Nucl. Mater. 4 (2012) 667–690. https://core.ac.uk/download/pdf/208176021.pdf.

[8] G. Carro, A. Muñoz, M.A. Monge, B. Savoini, R. Pareja, C. Ballesteros, P. Adeva, Fabrication and characterization of Y_2O_3 dispersion strengthened copper alloys, J. Nucl. Mater. 455 (1-3) (2014) 655–659, https://doi.org/10.1016/j.jnucmat.2014.08.050.

[9] G. Carro, A. Muñoz, M.A. Monge, B. Savoini, A. Galatanu, M. Galatanu, R. Pareja, Thermal conductivity and diffusivity of Cu-Y alloys produced by different powder metallurgy routes, Fusion Eng. Des. 124 (2017) 1156–1160, https://doi.org/10.1016/j.fusengdes.2017.01.017.

[10] G. Carro, A. Muñoz, B. Savoini, M.A. Monge, R. Pareja, Processing, microstructure and mechanical characterization of dispersion strengthened Cu-1%Y, Fusion Eng. Des. 138 (2019) 321–331, https://doi.org/10.1016/j.fusengdes.2018.11.058.

[11] S.M.S. Aghamiri, N. Oono, S. Ukai, R. Kasada, H. Noto, Y. Hishinuma, T. Muroga, Microstructure and Mechanical properties of mechanically alloyed ODS copper alloy for fusion material application, Nucl. Mater. Energy 15 (2018) 17–22, https://doi.org/10.1016/j.nme.2018.05.019.

[12] D. Zhou, H. Geng, W. Zeng, D. Zheng, H. Pan, C. Kong, P. Munroe, G. Sha, C. Suryanarayana, D. Zhang, High temperature stabilization of a nanostructured Cu-Y2O3 composite through microalloying with Ti, Mater. Sci. Eng., A 712 (2018) 80–87, https://doi.org/10.1016/j.msea.2017.11.105.

[13] A. Muñoz, B. Savoini, M.A. Monge, M. Eddahbi, O.J. Dura, Microstructure and mechanical properties of hot rolled ODS copper, Nucl. Mater. Energy 24 (2020) 100754, https://doi.org/10.1016/j.nme.2020.100754.

[14] K. Byungchul, J. Jinsung, K. Tae Kyu, A. Jung-Ho, Synthesis and properties of Ni/Y2O3 nanocomposites, Rev. Adv. Mater. Sci. 28 (2011) 166–170. http://194.226.210.10/e-journals/RAMS/no_22811/37_paper.pdf.

[15] J. Rodríguez-Carvajal, Recent advances in magnetic structure determination by neutron powder diffraction, Phys. B Condensed Matter. 192 (1-2) (1993) 55–69, https://doi.org/10.1016/0921-4526(93)90108-I.

[16] F. Bachmann, R. Hielscher, H. Schaeben, Grain detection from 2d and 3d EBSD data Specification of the MTEX algorithm, Ultramicroscopy 111 (12) (2011) 1720–1733, https://doi.org/10.1016/j.ultramic.2011.08.002.

[17] Y.-H. Xu, H.C. Pitot, An improved stereologic method for three-dimensional estimation of particle size distribution from observations in two dimensions and its application, Comput. Methods Programs Biomed. 72 (1) (2003) 1–20, https://doi.org/10.1016/S0169-2607(02)00115-3.

[18] F. Ribot, P. Toledano, C. Sanchez, X-Ray and spectroscopic investigations of the structure of yttrium acetate tetrahydrate, Inorg. Chim. Acta 185 (2) (1991) 239–245, https://doi.org/10.1016/S0020-1693(00)85449-3.

[19] J. Farjas, J. Camps, P. Roura, S. Ricart, T. Puig, X. Obradors, Thermoanalytical study of the formation mechanism of yttria from yttrium acetate, Thermochim. Acta 521 (1-2) (2011) 84–89, https://doi.org/10.1016/j.tca.2011.04.009.

[20] M.W., Jr. Chase, NIST-JANAF Thermochemical Tables, Fourth Edition, J. Phys. Chem. Ref. Data, Monograph 9 (1998) 1-1951.

[21] B.N. Singh, A. Horsewell, P. Toft, D.J. Edwards, Temperature and dose dependencies of microstructure and hardness of neutron irradiated OFHC copper,

J. Nucl. Mater. 224 (2) (1995) 131–140, https://doi.org/10.1016/0022-3115(95)00054-2.
[22] B. Huanga, Y. Hishinumaa, H. Noto, R. Kasada, N. Oono, S. Ukai, T. Muroga, In-situ fabrication of yttria dispersed copper alloys through MA-HIP process, Nucl. Mater. Energy 16 (2018) 168–174, https://doi.org/10.1016/j.nme.2018.06.024.
[23] T.J. Miller, S.J. Zinkle, B.A. Chin, Strength and fatigue of dispersion-strengthened copper, J. Nucl. Mater. 179–181 (1991) 263–266, https://doi.org/10.1016/0022-3115(91)90076-J.
[24] W. Gao, A. Belyakov, H. Miura, T. Sakai, "Dynamic recrystallization of copper polycrystals with different purities, Materials Science and Engineering A,265 (1999) 233-239. https://doi.org/10.106/S0921-5093(99)00004-0.
[25] Paul H. Sidles, G.C. Danielson, Thermal conductivity of metals at high temperatures, Ames Labor. ISC Tech. Rep. 36 (1951).
[26] G.K. White, S.J. Collocott, Heat capacity of reference materials: Cu and W, J. Phys. Chem. Ref. Data 13 (4) (1984) 1251–1257, https://doi.org/10.1063/1.555728.
[27] S.D. Preston, I. Bretherton, C.B.A. Forty, The thermophysical and mechanical properties of the copper heat sink material intended for use in ITER, Fusion Eng. Des. 66–68 (2003) 441–446, https://doi.org/10.1016/S0920-3796(03)00190-X.
[28] L. Yingguang, Z. Shingbing, H. Zhonghe, Z. Yujin, Grain-size-dependent thermal conductivity of nanocrystalline materials, J. Nanopart. Res. 18 (2016) 296, https://doi.org/10.1007/s11051-016-3606-8.